



Power Electronic Systems
Laboratory

© 2017 IEEE

Proceedings of the IEEE International Electric Machines & Drives Conference (IEMDC 2017), Miami, FL, USA, May 21-24, 2017

Homopolar Bearingless Slice Motor in Temple Design

P. Püntener,
F. Hoffmann,
D. Menzi,
D. Steinert,
J. W. Kolar

This material is published in order to provide access to research results of the Power Electronic Systems Laboratory / D-ITET / ETH Zurich. Internal or personal use of this material is permitted. However, permission to reprint/republish this material for advertising or promotional purposes or for creating new collective works for resale or redistribution must be obtained from the copyright holder. By choosing to view this document, you agree to all provisions of the copyright laws protecting it.



Eidgenössische Technische Hochschule Zürich
Swiss Federal Institute of Technology Zurich

Homopolar Bearingless Slice Motor in Temple Design

Pascal Puentener¹, Felix Hoffmann¹, David Menzi¹, Daniel Steinert², Johann W. Kolar¹

¹Power Electronic Systems Laboratory, ETH Zurich, Zurich, Switzerland

²Levitronix GmbH, Zurich, Switzerland

Abstract—This work describes a concept of a magnetically levitated homopolar bearingless slice motor in temple design. The proposed setup consists of two oppositely magnetized permanent magnets on the rotor and stator and provides high axial stiffness. The fluctuation of the air gap field for torque generation is generated with a cross-shaped rotor iron. Compared to a diametrically magnetized drive, this concept achieves three times the axial stiffness without increasing the radial stiffness and is better suited for systems with large air gaps. A drawback is the low torque capacity. Its operating principle is described and a working prototype is presented including simulation and measurement results.

Keywords—bearingless motor, homopolar bearing, passive stiffness.

I. INTRODUCTION

Bearingless motors were introduced in the early 1990 [1], [2]. Thanks to the integration of the bearing and drive in a single magnetic circuit, it also allows for a compact design. An even more compact and simpler design can be achieved if the rotor height is smaller than its diameter [3]. These slice motors are passively stable in three directions and are used in industrial applications such as high-purity pumps [4], [5], blowers [6] and artificial hearts [7], [8]. Such drives are usually designed with large air gaps. For high-purity pump applications the air gap is required to hermetically seal the fluid by inserting a process chamber. In medical applications, a larger air gap causes less cell damage and can provide a long term support of the heart.

One of the major challenges that are associated with large air gaps is the passive stiffness of the bearing. During operation high process forces must be compensated by the reluctance force as exemplary illustrated in Fig. 1 with of a hermetically sealed pump. With increasing distance between the rotor and the stator wall the achievable forces of the bearing are decreased. This becomes problematic if a minimal air gap is required due to manufacturing tolerances or demanded by the application.

To achieve a high axial stiffness, homopolar bearingless motors can be used which were already introduced in [9] and patent-registered [10]. Permanent magnets on the rotor and stator side provide a biased flux in the air gap and can achieve

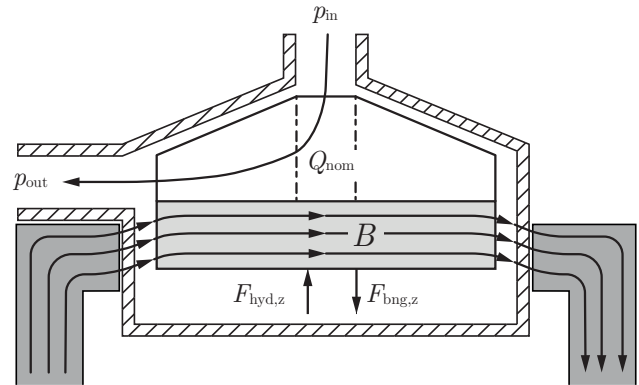


Fig. 1. Schematics of a bearingless pump with pump housing (shaded). Due to different pressure distribution between the bottom and upper part of the impeller an axial force $F_{\text{hyd},z}$ results. This leads to a displacement z of the rotor in axial direction towards the equilibrium position where the reluctance force of the bearing $F_{\text{bng},z}$ compensates the hydraulic force.

higher passive stiffnesses than commonly used diametrically magnetized slice motors presented in [11]. An alternating field required to generate torque can be generated if the permanent magnets on the rotor are placed with a distance in between them.

Unfortunately, this concept is not available for small sized systems so far. Furthermore, to operate such a motor as a centrifugal pump or blower, an outlet is required where the fluid can leave the housing. The flat design of the stator does not allow for such an exit as the space is occupied by the windings.

A much more favorable topology is the so-called temple design [12] which has its windings distributed in axial direction, leaving space for an outlet. A homopolar version of such a temple design with permanent magnet free rotor was introduced in [13]. This motor has the permanent magnet located on the stator in the middle of the machine. It also requires a collection plate centered in the middle of the ring-shaped rotor. As a result, a hermetical sealing of such a system is more complicated because it exhibits two air gaps and the rotor shape is limited to be a ring with salient poles. Furthermore, the achievable axial stiffness is considerably lower.

In this work, a concept that provides a high axial stiffness

This work was supported by the Swiss Commission for Technology and Innovation CTI-KTI.

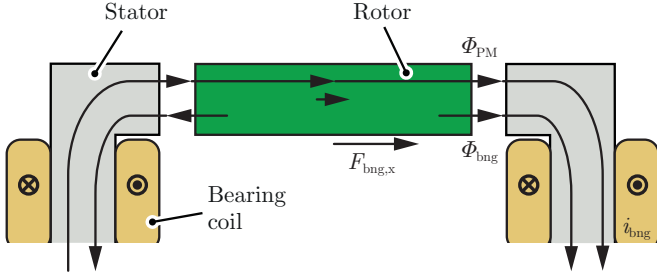


Fig. 2. Principle of a diametrically magnetized bearingless drive. The rotor creates a magnetic field with pole pair number one ($p = 1$). Opposite windings need to be excited in the same direction to generate a bearing force. The PM flux and the drive/bearing fields occupy the same magnetic path. The bearing flux closes its path over the neighboring stator tooth (not shown).

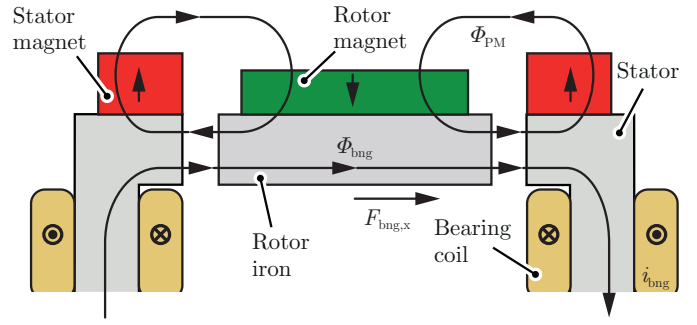


Fig. 3. Principle of the homopolar bearingless motor in temple design. The rotor PM creates a magnetic field which is divided by the rotor iron into an even pole pair number with DC offset. In order to generate bearing forces opposite windings need to be excited in opposite directions. The PM flux mainly passes through the air above the motor and is only in the stator teeth and parts of the rotor iron aligned with the drive and bearing field lines.

and can overcome the aforementioned problems is presented. Its operating principle and the superior passive characteristics are presented in section II and III. It is shown in section V that this concept offers better passive properties for large air gaps than diametrically magnetized topologies. Finally, the design and results of a working prototype are presented in section VI and VII.

II. CONCEPT

The concept presented here is based on the magnetically levitated homopolar motor (MHM) presented in [9] and the temple motor design [12]. Three degrees of freedom (DOF) of the rotor are stabilized passively, namely the axial displacement and tilting around the x - and y -axis. The remaining three DOF are actively controlled by the bearing (radial displacement) and drive (rotor angle around the axis of rotation).

Similar to the MHM, contrarily magnetized permanent magnets (PMs) on the stator and the rotor stabilize tilting and axial deflections of the rotor [11]. However, instead of using several rotor magnets that are spatially separated, a rotor iron with varying reluctance across its circumference is attached underneath a single rotor magnet. This generates the fluctuating B -field in the air gap which is required to generate a torque. The iron is also used to bend the magnetic flux radially towards the stator teeth.

Fig. 2 and Fig. 3 show a schematic comparison between the diametrically magnetized and the homopolar bearingless temple motor. While the diametrical concept only uses a permanent magnet on the rotor, the homopolar concept also contains PMs on the stator.

The diametrically magnetized rotor closes its magnetic path through the stator iron, whereas the B -field of the homopolar concept concentrates in the upper part of the stator iron and closes the path in the air above the motor. Fig. 4 shows a FEM simulation of the B -field generated by the PMs. Near the PM edges, some saturation effects can be observed. The lower part of the stator and rotor iron remain unsaturated, providing a high permeability for the drive and bearing fluxes.

Fig. 5 shows a top view of the B -field in the air gap for a cross shaped rotor iron. The field is concentrated near the

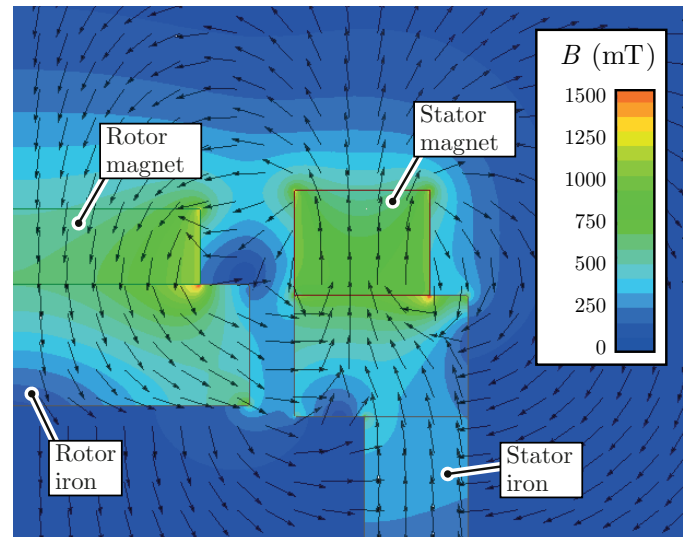


Fig. 4. Magnetostatic FEM simulation of the homopolar bearingless motor. The major part of the flux passes through the air above the machine and is directed radially in the air gap. The flux passes through the upper part of the rotor- and stator iron. The lower part remains field free and can be used by the driving- and bearing field. Due to the high permeability of the rotor iron, the magnetic air gap can be reduced significantly compared to a diametrically magnetized system.

rotor iron tips. A field with four pole pairs results that can be used to generate a drive torque. Its DC offset is used to generate bearing forces.

Throughout this paper, a cross shaped rotor iron with pole pair number four is analyzed. More elaborated iron shapes, that provide a more sinusoidal flux density distribution in the air gap, are listed in [10]. Due to the simple machining of iron, almost no boundaries to the shape are set.

III. PASSIVE CHARACTERISTICS

A. Axial Stiffness

The passive stiffnesses of bearingless drives are important characteristics. They limit the process forces that can be withstand. For pump applications, the most important quantity

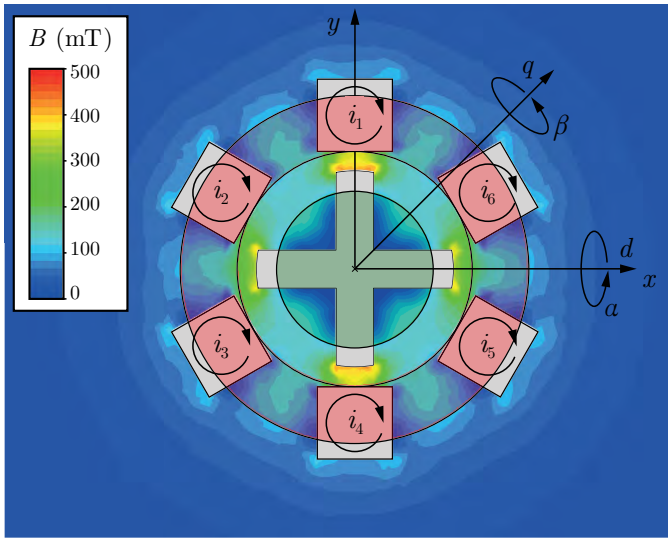


Fig. 5. Magnetostatic FEM simulation showing the top view of the air gap field. Rotor iron (cross), rotor PM (circle), stator claws (squares) and stator PM (ring). The lower magnetic reluctance through the rotor iron concentrates the air gap field near the rotor tips. For the illustrated topology, a magnetic field with pole pair number $p = 4$ and DC offset results.

is the axial stiffness k_z as it limits the maximal pressure that can be handled.

It is defined as the change in axial force $F_{\text{bng},z}$ with respect to an axial displacement z of the rotor

$$k_z = -\frac{dF_{\text{bng},z}}{dz} > 0. \quad (1)$$

Fig. 6(a) shows a schematic drawing of the system in a cross sectional view. If the rotor is displaced in z -direction, the distance between the rotor and the stator is increased. The resulting reluctance force $F_{\text{bng},z}$ attracts the rotor back to the equilibrium point.

B. Radial Stiffness

As described in [14], a positive axial stiffness results in a destabilizing radial stiffness, that is at least half as large in magnitude

$$|k_r| = \left| \frac{dF_r}{dr} \right| > \frac{1}{2} |k_z|, \quad (2)$$

where k_r is the radial stiffness.

As the radial stiffness destabilizes the rotor, it is favorable to achieve low values of $|k_r|$, such that the control loop of the bearing can be slower and disturbances have a lower impact.

Therefore, a good design is striving for a low ratio of $|k_r/k_z|$. As described in [14], the ratio is minimized to 1/2 if solely permanent magnets are used. Considering the flux path of the PMs in this design, it becomes apparent that the magnetic field requires to penetrate a lot of air. As a consequence, the ratio is expected to be better for the presented concept than for diametrically magnetized ones.

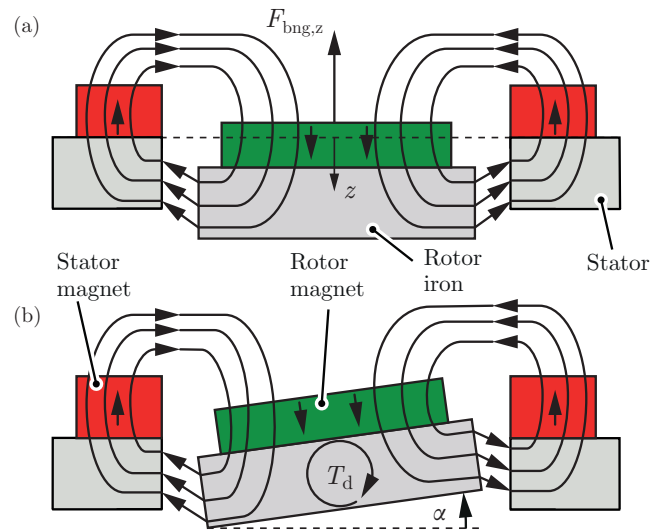


Fig. 6. Axial (a) and tilting displacements (b) of the rotor from its equilibrium position. Reluctance forces $F_{\text{bng},z}$ and torques T_d counteract the rotor displacement.

C. Tilting Stiffness

The tilting stiffness of a bearingless motor is defined as the change in restoring torque acting on the rotor due to a tilting of the rotor around any radial direction. It has to be distinguished between rotations around the d - and the q -axis as illustrated in Fig. 5

$$k_\alpha = -\frac{dT_d}{d\alpha} \quad k_\beta = -\frac{dT_q}{d\beta}. \quad (3)$$

Due to the concentration of the flux density at the rotor tips, the tilting stiffness around the d -axis k_α is lower than k_β .

A schematic drawing of a tilted rotor is illustrated in Fig. 6(b). Similar to the case of an axial displacement, the air gap is increased if the rotor tilts. The resulting reluctance forces cause the rotor to be pulled back to its center position.

For topologies exhibiting a slotted stator, these stiffnesses are functions of the rotor angle φ . The minimum value is of major interest as it is required to be positive for stable operation. It is desirable to achieve a high tilting stiffness as this will result in a system that tends less to a tilting movement.

It will be shown in a later section, that the tilting stiffness can be influenced largely by the height of the rotor PM. Though, it remains a trade-off between a high axial and tilting stiffness.

IV. ACTIVE CHARACTERISTICS

A. Radial Bearing

As the rotor generates a biased magnetic field, bearing forces can be generated by strengthening the magnetic field in one direction and weakening it on the other side. This causes the rotor to be attracted towards the side with higher flux density.

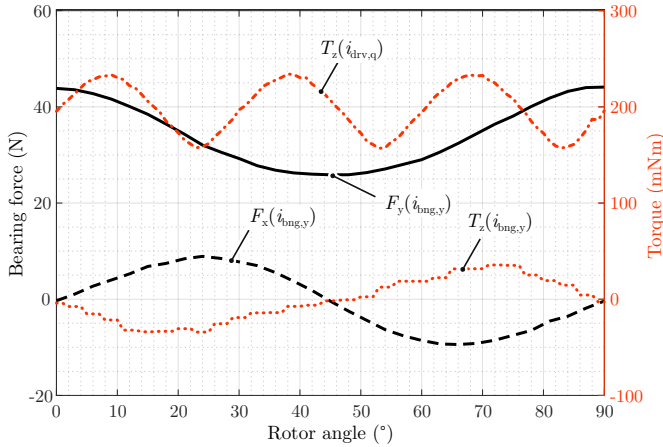


Fig. 7. Force generation for a rotation of the rotor by 90° and a bearing current of $\hat{I}_{\text{bng}} = 5 \text{ A}$ generating a bearing force in y -direction. Resulting force in y -direction (solid black) and x -direction (dashed black) as well as the torque (dotted red) caused by the coupling. For the same rotation of the rotor but pure q -current (drive current) of $\hat{I}_{\text{drv}} = 5 \text{ A}$ the resulting torque also shows a fluctuation (dash-dotted red).

If the directions of the current are defined such that they excite a magnetic field in the air gap pointing outward (i.e. in a clock-wise manner in Fig. 5), the resulting bearing forces can be described as

$$\vec{F}_{\text{bng},r} = F_{\text{bng}} \begin{pmatrix} -\sin(\varphi_{\text{bng}}) \\ \cos(\varphi_{\text{bng}}) \end{pmatrix} = k_{\text{I}} \cdot \vec{i}_{\text{bng}}, \quad (4)$$

with

$$\vec{i}_{\text{bng}} = \begin{pmatrix} (i_2 + i_3 - i_5 - i_6) \sin(\pi/3) \\ i_1 - i_4 + (i_2 + i_6 - i_3 - i_5) \cos(\pi/3) \end{pmatrix} \quad (5)$$

and

$$i_k = \hat{I}_{\text{bng}} \cos\left(\varphi_{\text{bng}} - \frac{k\pi}{3}\right), \quad k \in \{1, 6\}, \quad (6)$$

where the indices coincide with the notation of Fig. 5.

Equation (4) shows that the bearing forces can be generated without knowledge of the rotor angle. This fact is a clear advantage common to homopolar bearings compared to diametrically magnetized rotors. The control becomes much simpler and no angle information is required for a stable levitation.

Due to the fluctuating B -field required by the drive, the radial force generation is not independent of the rotor angle. Figure 7 illustrates the generated bearing force for a current excitation in y -direction and a rotation of the rotor by 90° . The desired force in y -direction fluctuates by approximately 25%. At the same time an undesired force in x -direction is generated with the same fluctuation. To achieve good bearing properties, a sufficiently fast control loop or a compensation of the force fluctuation is required.

It can also be seen in Fig. 7 that the force generation is coupled with a torque. For the considered topology, a desired force of 35 N causes a torque fluctuation with a magnitude of 30 mNm (dashed blue). If a precise torque generation is required, the coupling would have to be taken into account

by the controller. A complete rotor angle independent force generation could be achieved if the width of the stator teeth is chosen such that it covers an entire electric period of the rotor field [9]. However, this would require the rotor pole pair number to be larger than the stator one.

B. Torque Generation

The principle of the drive is the same as for any permanent magnet synchronous motor. A magnetic field with pole pair number equal to the rotor one is required to generate a torque. This can be achieved by exciting the drive coils according to

$$i_k = \hat{I}_{\text{drv}} \cos\left(\varphi_{\text{drv}} + 4\left(\varphi - \frac{k\pi}{3}\right)\right), \quad k \in \{1, 6\}, \quad (7)$$

where φ_{drv} , φ are the drive and rotor angle, respectively. The indices coincide with the notation of Fig. 5.

Due to the high permeability of the rotor iron, the magnetic flux density and, therefore, the torque highly depend on the rotor angle. Figure 7 shows the torque generation (solid blue) for a rotating rotor if pure q -current is applied. The nominal value is achieved whenever an iron tip points towards a stator claw. For the considered topology, the peak-to-peak value of this fluctuation is 38% of the mean torque magnitude.

The high torque characteristics of diametrically magnetized rotors cannot be achieved with this topology, independent of the rotor iron shape. This is due to the lower fluctuation of the magnetic field in the air gap. Typically, homopolar motors achieve no more than half the torque of a similar diametrical motor due to the lack of a change in the direction of the magnetic flux density.

V. SCALING PROPERTIES

Given a certain system and using FEM simulations, it is possible to predict the properties of a drive with larger or smaller size. To do so, all dimensions are scaled by a factor x_{d} and the resulting characteristics are compared to the properties of the initial system.

An advantage of the proposed concept is its superior down-scaling behavior ($x_{\text{d}} < 1$) compared to diametrically magnetized concepts. Due to a relatively small contribution of the radial air gap to the overall reluctance in the PMs flux path, an increasing radial gap is less pronounced than for a diametrical system.

A. Proportional Scaling

As described in [15], the transversal passive stiffnesses do scale linearly with the dimension and the axial bearing force scales quadratically:

$$k_z \propto x_{\text{d}}, \quad F_{\text{bng},z} \propto x_{\text{d}}^2. \quad (8)$$

This is the case for any bearingless motor, regardless of its topology. Typically, the arising process forces also become smaller with decreasing device size. For example, the hydraulic axial force $F_{\text{hyd},z}$ acting on the impeller of a pump scales quadratically with x_{d} [16]. Therefore, an axially stable operation can be achieved regardless of the size of the pump, as long as all dimensions are scaled equally.

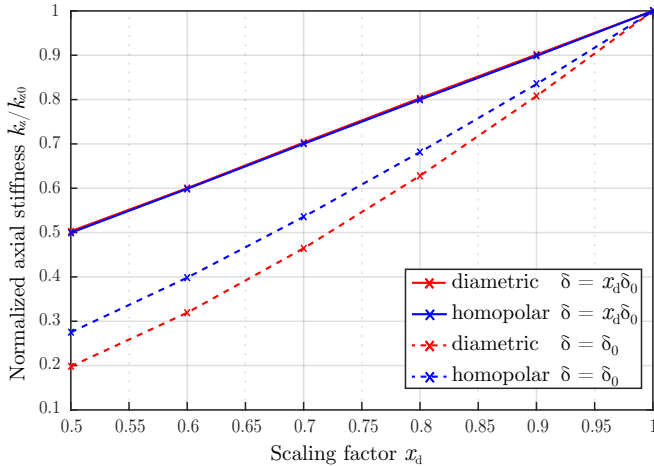


Fig. 8. Simulation of the change in axial stiffness of the two concepts when reducing the overall system size. Red: diametrically magnetized, blue: homopolar concept. Solid lines: variable air gap, dashed lines: constant air gap.

B. Scaling with Constant Air Gap

Problems arise if the air gap of a bearingless system must retain a minimal length or shall be increased, e.g. in case a pump head requires a minimal wall thickness in order to withstand the pressure at the impeller outlet. The previously presented scaling laws are no longer valid. In such a case, the air gap length must be increased relative to the system dimensions during down-scaling. Consequently, the magnetic flux density in the radial gap decreases and the bearing stiffnesses drop more rapidly

$$\frac{\partial k_z}{\partial x_d} > 1. \quad (9)$$

This in turn constrains the maximum process force the system can bear and consequently the operational range.

The rate $\frac{\partial k_z}{\partial x_d}$ at which the axial stiffness reduces when down-scaling the system depends on the topology of the motor. FEM simulations were performed to verify that the proposed concept achieves lower values of $\frac{\partial k_z}{\partial x_d}$. The results are presented in Fig. 8. Compared to the diametrically magnetized concept, the loss in axial stiffness can be reduced for the case that the air gap length is increased relative to the system size. Down-scaling by a factor of two while keeping the air gap at the same length reduces the axial stiffness of the diametrically magnetized system by 80%. For the presented homopolar motor the axial stiffness is reduced by only 73%. Hence, this topology is well suited for applications that require large air gaps and a high axial stiffness.

VI. PROTOTYPE

To proof the concept of the homopolar bearingless temple motor, a prototype was built by adjusting the stator of an existing bearingless slice motor.

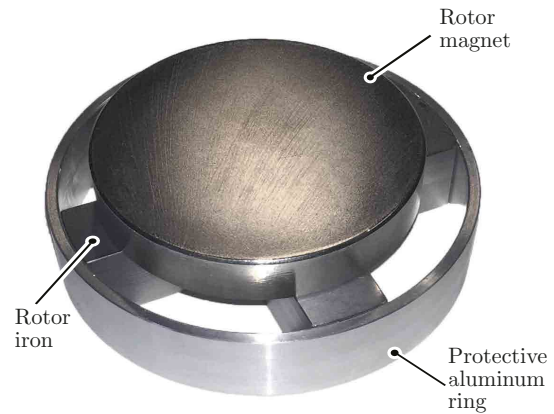


Fig. 9. Assembly of the rotor consisting of an axially magnetized magnet (top), cross-shaped rotor iron (center bottom) and an aluminum ring to protect the stator.

A. Rotor

An axially magnetized NdFeB PM with diameter $D_{pm} = 60$ mm was used for the rotor. A cross-shaped rotor iron is attached below the PM, as illustrated in Fig. 9, to guide the flux with pole pair number $p = 4$ radially towards the stator teeth. The diameter of the rotor iron was chosen equal to the rotor diameter of the diametrically magnetized reference rotor, to achieve comparability.

Fig. 10 shows the axial and tilting stiffnesses as a function of the rotor PM height with otherwise constant parameters. Both stiffnesses achieve a clear maximum. The maximal axial stiffness is achieved for a magnet height of 17 mm. However, for such a high rotor, the system becomes unstable in tilting direction as indicated by the dashed red line. The maximum tilting stiffness on is achieved when the axial stiffness is comparatively low. For the prototype, a rotor PM height of $H_{pm} = 10$ mm was chosen as a trade-off for a simultaneously high axial and tilting stiffness.

To protect the stator from destruction in case the rotor becomes unstable and touches the stator wall, the iron cross was covered by an aluminum ring.

B. Stator

A stator in temple design with six stator claws was used. A ring shaped NdFeB magnet with outer diameter $D_{out} = 110$ mm, inner diameter $D_{in} = 75$ mm and height $H = 14$ mm was mounted on top of the stator to achieve a high axial stiffness and a similar radial stiffness as the diametrically magnetized rotor used as a reference. A photograph of the assembled prototype is shown in Fig. 11.

The bearing and drive coils were each realized using a three phase system with floating star point. The supplying dc voltage was 325 V. Windings on opposite sides were connected in series but with different winding orientation for bearing and drive.

VII. RESULTS

A summary of the motor properties and a comparison to a diametrically magnetized system is given in Table I

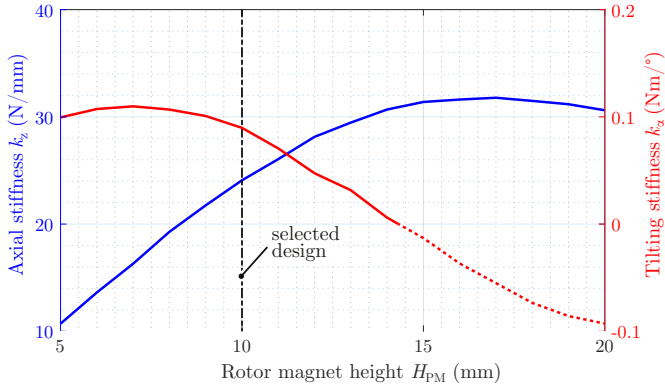


Fig. 10. Axial (blue) and tilting stiffness (red) as a function of the rotor PM height. The dashed part indicates the unstable region. The design parameter selected for the prototype is marked by the vertical dashed line.

A. Axial Stiffness

The prototype achieved an axial stiffness of $k_z = 23.9 \text{ N/mm}$. Measurements coincide well with the simulation results $k_{z,\text{sim}} = 23.2 \text{ N/mm}$. Compared to a diametrically magnetized rotor with similar dimensions ($k_z = 7.2 \text{ N/mm}$) the axial stiffness could be increased by a factor of 3.3.

B. Radial Stiffness

The prototype was designed such that it achieves the same radial stiffness as a diametrically magnetized motor. As a result, the radial stiffness remains nearly unchanged and is $k_r = -24.9 \text{ N/mm}$.

As expected, the ratio $|k_r/k_z|$ could be reduced by more than a factor of 3 from 3.6 to 1.04. This is due to the much higher reluctance in the flux path of the PM above the motor and the lower amount of permeable material.

C. Tilting Stiffness

At the same time the tilting stiffness was increased from $k_{\alpha} = 81 \text{ mNm/}^\circ$ and $k_{\beta} = 33.4 \text{ mNm/}^\circ$ to $k_{\alpha} = 211 \text{ mNm/}^\circ$ and $k_{\beta} = 175 \text{ mNm/}^\circ$, respectively.

For the weak tilting axis, this is an increase by a factor of 5.2. Due to the higher pole pair number, the tilting stiffness was also homogenized. Therefore, the rotor has a lower tendency to tilt along a certain axis.

D. Torque

As a consequence of the biased air gap field, the torque capacity drops significantly. Compared to the diametrically magnetized rotor, the peak to peak value of the radial B -field in the air gap was reduced from 1.6 T to 0.25 T. However, due to the much lower reluctance, the torque constant k_T only reduces by a factor of 3.5.

Furthermore, the prototype was successfully operated up to 5000 rpm in air and could also be operated as a pump.

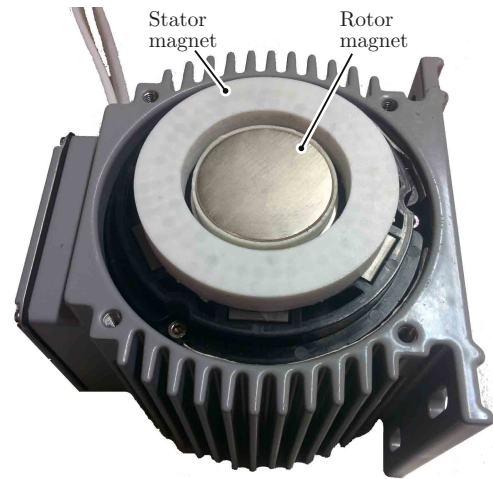


Fig. 11. Assembled prototype with levitating rotor. The stator magnet ring (white) can simply be added to the stator.

TABLE I
COMPARISON OF THE CHARACTERISTICS

Parameter	Homopolar	Diametrical	Unit
axial stiffness, k_z	23.9	7.2	N/mm
radial stiffness, k_r	-24.9	-25.9	N/mm
ratio $ k_r/k_z $	1.04	3.6	—
tilting stiffness around d , k_{α}	175	33.4	mNm/°
tilting stiffness around q , k_{β}	211	81	mNm/°
ratio $ k_{\alpha}/k_{\beta} $	0.83	0.41	—
torque constant, k_T	34	120	mNm/A
torque at $\hat{I}_{\text{drv}} = 5 \text{ A}$, T_{sat}	0.15	0.6	Nm

VIII. CONCLUSION

Based on the principle of the magnetically levitated homopolar motor [9] and the temple topology [12] a novel homopolar bearingless drive was developed. The motor consists of oppositely magnetized permanent magnets on the rotor and stator side. The axial and tilting movements are stabilized passively by means of repelling reluctance forces. A cross-shaped iron was attached below the permanent magnet of the rotor to guide the flux density towards the stator teeth. A varying reluctance along its circumference generates the periodic fluctuation required by the drive.

Using FEM simulations it was shown that this concept can achieve a higher axial stiffness than a comparable diametrically magnetized system. To proof the concept, a prototype was built and tested successfully. Compared to a diametrically magnetized rotor the axial stiffness could be increased by a factor of 3.3, while keeping the radial stiffness unchanged. Also, the tilting stiffness could be increased by at least a factor of 2.5. The major drawbacks are its low torque capability, high torque and force ripples and the required total permanent magnet volume.

It was simulated that the new concept is superior if a minimal air gap length needs to be maintained. Therefore, this topology fits best for applications with a large air gap and high process forces but lower torque requirements.

REFERENCES

- [1] J. Bichsel, "The bearingless electrical machine," in Proc. ISMST. NASA, Langley Research Center, May 1992, pp. 561–573.
- [2] A. Chiba, D. T. Power, and M. A. Rahman, "Characteristics of a bearingless induction motor," IEEE Transactions on Magnetics, vol. 27, no. 6, pp. 5199–5201, Nov 1991.
- [3] R. Schoeb and N. Barletta, "Magnetic bearing. principle and application of a bearingless slice motor." JSME International Journal Series C Mechanical Systems, Machine Elements and Manufacturing, vol. 40, no. 4, pp. 593–598, 1997.
- [4] J. Asama, D. Kanehara, T. Oiwa, and A. Chiba, "Development of a compact centrifugal pump with a two-axis actively positioned consequent-pole bearingless motor," IEEE Transactions on Industry Applications, vol. 50, no. 1, pp. 288–295, 2014.
- [5] M. Neff, N. Barletta, and R. Schoeb, "Bearingless centrifugal pump for highly pure chemicals," in Proc. 8th ISMB, 2002, pp. 283–287.
- [6] R. Baumschlager, R. Schoeb, and J. Schmied, "Bearingless hydrogen blower," in Proc. on 8th ISMB Int. Symposium on Magnetic Bearings, 2002.
- [7] H. M. Loree, K. Bourque, D. B. Gernes, J. S. Richardson, V. L. Poirier, N. Barletta, A. Fleischli, G. Foiera, T. M. Gempp, R. Schoeb et al., "The heartmate iii: design and in vivo studies of a maglev centrifugal left ventricular assist device," Artificial organs, vol. 25, no. 5, pp. 386–391, 2001.
- [8] J. Asama, T. Fukao, A. Chiba, A. Rahman, and T. Oiwa, "A design consideration of a novel bearingless disk motor for artificial hearts," in 2009 IEEE Energy Conversion Congress and Exposition. IEEE, 2009, pp. 1693–1699.
- [9] T. Schneeberger, T. Nussbaumer, and J. W. Kolar, "Magnetically levitated homopolar hollow-shaft motor," IEEE/ASME Transactions on Mechatronics, vol. 15, no. 1, pp. 97–107, 2010.
- [10] R. Schoeb, "Magnetically journalled rotational arrangement including a rotor for generating a unipolar bias magnetic flux," U.S. Patent 7,112,903 B1, Sep 26, 2006.
- [11] T. Nussbaumer, P. Karutz, F. Zurcher, and J. W. Kolar, "Magnetically levitated slice motors - an overview," IEEE Transactions on Industry Applications, vol. 47, no. 2, pp. 754–766, 2011.
- [12] N. Barletta and R. Schoeb, "Design of a bearingless blood pump," 1996.
- [13] W. Gruber, M. Rothböck, and R. T. Schoeb, "Design of a novel homopolar bearingless slice motor with reluctance rotor," IEEE Transactions on Industry Applications, vol. 51, no. 2, pp. 1456–1464, 2015.
- [14] J.-P. Yonnet, "Permanent magnet bearings and couplings," IEEE Transactions on Magnetics, vol. 17, no. 1, pp. 1169–1173, 1981.
- [15] D. Steinert, T. Nussbaumer, and J. W. Kolar, "Concept of a 150 krpm bearingless slotless disc drive with combined windings," in Electric Machines & Drives Conference (IEMDC), 2013 IEEE International. IEEE, 2013, pp. 311–318.
- [16] H. M. Badr and W. H. Ahmed, Pumping Machinery Theory and Practice. John Wiley & Sons Ltd, 2014, ch. Axial and Radial Thrusts in Centrifugal Pumps, pp. 133–158.